

Simulated single molecule microscopy with SMeagol

Martin Lindén, Vladimir Ćurić, Alexis Boucharin, David Fange, & Johan Elf[†]

Department of Cell and Molecular Biology, Uppsala University, Sweden. [†]johan.elf@icm.uu.se

Summary: SMeagol is a software tool to simulate highly realistic microscopy data based on spatial systems biology models, in order to facilitate development, validation, and optimization of advanced analysis methods for live cell single molecule microscopy data.

Availability and Implementation: SMeagol runs on Matlab R2014 and later, and uses compiled binaries in C for reaction-diffusion simulations. Documentation, source code, and binaries for recent versions of Mac OS, Windows, and Ubuntu Linux can be downloaded from

<http://smeagol.sourceforge.net>.

Supplementary information: Supplementary data are available at *Bioinformatics* online.

Recent advances in single particle tracking (SPT) microscopy¹ make it possible to obtain tens of thousands macromolecular trajectories from within a living cell in just a few minutes. Since molecules typically change their movement properties upon interactions, these trajectories contain information about both locations and rates of intracellular reactions. This information is unfortunately obscured by physical limitations of the optical microscope and noise in detection systems, making statistical methods development for SPT analysis a very active research field. Unbiased testing and comparison of such methods are however difficult given the absence of in vivo data of intracellular dynamics where the true states of interaction are known, a.k.a. the ground truth. A common resort is to instead use simulated, synthetic, data. However, tests using such data give unrealistically optimistic results if the simplifying assumptions underlying the analysis method are exactly satisfied. The need for realistic simulations is long recognized in microscopy and systems biology^{2–12}, but systematic combinations of the two are only currently emerging^{13,14}.

We present the SMeagol package, that has been developed to generate highly realistic single molecule microscopy time-lapse image series aimed primarily at single particle tracking applications. The purpose of SMeagol is to enable realistic comparisons between the output of advanced analysis methods and known ground truth. SMeagol includes an extended MesoRD¹¹ version for simulation of 3D diffusion in cellular compartments, diffusion limited reaction kinetics, surface adsorption, reactions in membranes, and other complex aspects of reaction diffusion kinetics that do occur in cells, but are not considered in SPT analysis algorithms. In addition to the molecules' trajectories, SMeagol integrates the 3D point spread function of the microscope, the kinetics of photo-activation, blinking and bleaching of the simulated fluorophores, background noise, and camera specific parameters (Figure 1, movie S1,S2). Great flexibility is allowed by the possibility to supply these characteristic parameters either as tabulated experimental data for a particular optical setup, or as theoretical models. The combination of using reaction diffusion kinetics in cellular geometries and physics-based simulations of the emission and detection processes makes the images more realistic than the synthetic data used for example by⁵.

SMeagol can be used to optimize imaging conditions for specific systems in silico and to

benchmark methods for SPT analysis in analogy with the methods that has been developed to benchmark localization methods for non-moving single particles⁷. In the supplementary material, we explore the robustness against localization errors and motional blur of the vbSPT software, which extracts multi-state diffusive models from SPT data¹⁵, and find that these effects can induce overfitting under certain conditions. In addition, we provide a number of examples highlighting possibilities, limitation and computational requirements of the SMeagol simulation engine.

When combined with increasingly refined simulations of intracellular processes, photo-physics and optics; live-cell microscopy is moving closer to methods in fundamental physics, where combined simulation of physical processes and detection systems have guided experimental design and data analysis for a long time.

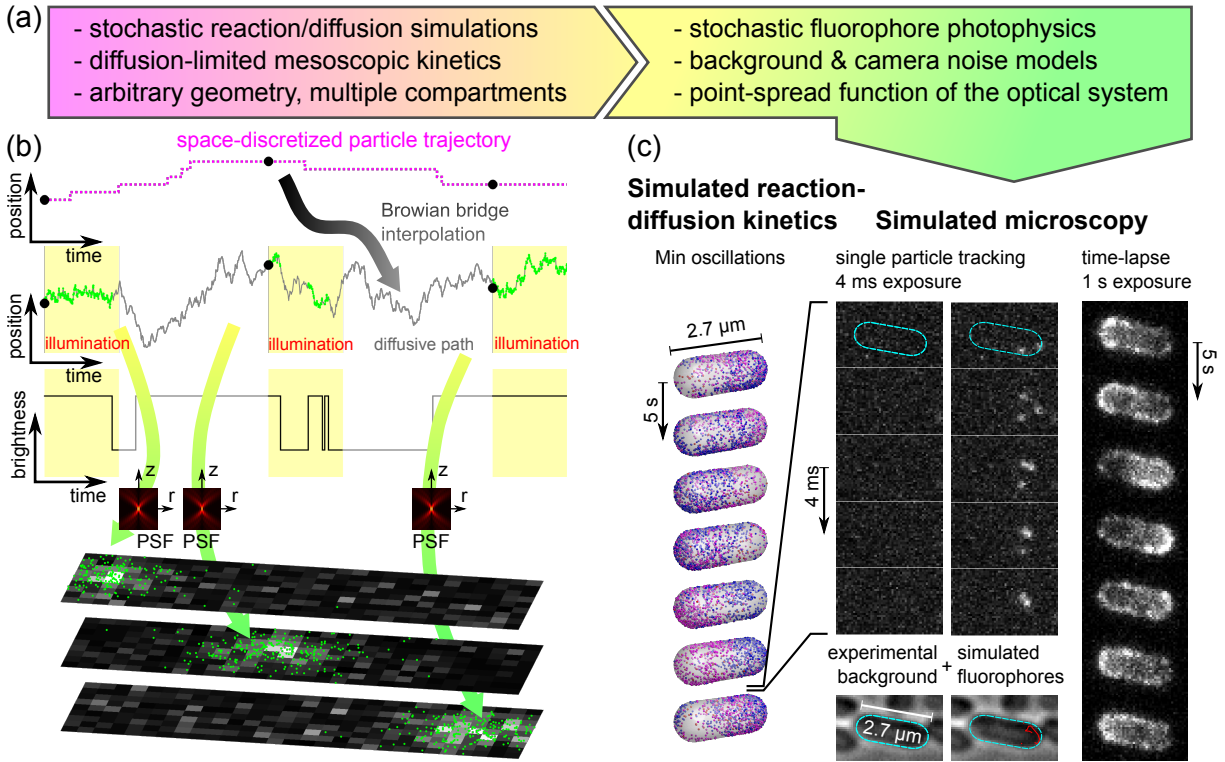


Figure 1: Simulated microscopy with SMeagol. (a) Workflow from stochastic reaction-diffusion simulations to images. (b) The microscopy simulation starts from trajectories generated by stochastic reaction-diffusion simulations, fills in stochastic motion and photon emission events between the trajectory points, and finally combines PSF and camera noise models to simulate realistic images. (c) Simulated microscopy of fluorescently labeled MinE proteins in the Min oscillatory system. Left: Stochastic reaction-diffusion simulation. Mid columns: Simulated SPT microscopy using an actual experimental background noise movie with continuous illumination and 4 ms/frame. Right: A simulation of continuous illumination and 1 s/frame renders a conventional (non-single molecule) fluorescence microscopy time-lapse movie. See also Supplementary movies S1,S2, and the Supplementary material for further details.

Acknowledgements

We thank Fredrik Persson and Elias Amselem for helpful discussions about microscopy.

Funding

This work was supported by the European Research Council, Vetenskapsrådet, the Knut and Alice Wallenberg Foundation, the Foundation for Strategic Research, and the Swedish strategic research programme eSSSENCE.

References

1. Suliana Manley, Jennifer M. Gillette, George H. Patterson, Hari Shroff, Harald F. Hess, Eric Betzig, and Jennifer Lippincott-Schwartz. High-density mapping of single-molecule trajectories with photoactivated localization microscopy. *Nat. Meth.*, 5(2):155–157, 2008. doi:10.1038/nmeth.1176.
2. Stephanie Fullerton, Keith Bennett, Eiji Toda, and Teruo Takahashi. Camera simulation engine enables efficient system optimization for super-resolution imaging. volume 8228 of *Proc. SPIE*, pages 822811–7, 2012. doi:10.1117/12.906346.
3. Tristan S. Ursell, Eliane H. Trepagnier, Kerwyn Casey Huang, and Julie A. Theriot. Analysis of surface protein expression reveals the growth pattern of the gram-negative outer membrane. *PLoS Comput. Biol.*, 8(9):e1002680, 2012. doi:10.1371/journal.pcbi.1002680.
4. Cox, S. *et al.* Bayesian localization microscopy reveals nanoscale podosome dynamics. *Nat. Meth.*, 9(2):195–200, 2012. doi:10.1038/nmeth.1812.
5. Chenouard, N. *et al.* Objective comparison of particle tracking methods. *Nat. Meth.*, 11(3):281–289, 2014. doi:10.1038/nmeth.2808.
6. Jzsef Sink, Rbert Kkonyi, Eric Rees, Daniel Metcalf, Alex E. Knight, Clemens F. Kaminski, Gbor Szab, and Mikls Erdlyi. TestSTORM: Simulator for optimizing sample labeling and image acquisition in localization based super-resolution microscopy. *Biomed. Opt. Express*, 5(3):778–787, 2014. doi:10.1364/BOE.5.000778.
7. Daniel Sage, Hagai Kirshner, Thomas Pengo, Nico Stuurman, Junhong Min, Suliana Manley, and Michael Unser. Quantitative evaluation of software packages for single-molecule localization microscopy. *Nat. Meth.*, 12(8):717–724, 2015. doi:10.1038/nmeth.3442.
8. Boris M. Slepchenko, James C. Schaff, John H. Carson, and Leslie M. Loew. Computational cell biology: spatiotemporal simulation of cellular events. *Annu. Rev. Biophys. Biomol. Struct.*, 31:423–441, 2002. doi:10.1146/annurev.biophys.31.101101.140930.
9. Rex A. Kerr, Thomas M. Bartol, Boris Kaminsky, Markus Dittrich, Jen-Chien Jack Chang, Scott B. Baden, Terrence J. Sejnowski, and Joel R. Stiles. Fast Monte Carlo simulation methods for biological reaction-diffusion systems in solution and on surfaces. *SIAM J. Sci. Comput.*, 30(6):3126–3149, 2008. doi:10.1137/070692017.

10. K. Takahashi, S. Tanase-Nicola, and P. R. ten Wolde. Spatio-temporal correlations can drastically change the response of a MAPK pathway. *Proc. Natl. Acad. Sci. U.S.A.*, 107(6):2473–2478, 2010. doi:10.1073/pnas.0906885107.
11. D. Fange, A. Mahmutovic, and J. Elf. MesoRD 1.0: Stochastic reaction-diffusion simulations in the microscopic limit. *Bioinformatics*, 28(23):3155–3157, 2012. doi:10.1093/bioinformatics/bts584.
12. Steven S. Andrews. Spatial and stochastic cellular modeling with the Smoldyn simulator. In Jacques van Helden, Ariane Toussaint, and Denis Thieffry, editors, *Bacterial Molecular Networks*, volume 804, pages 519–542. Springer, New York, NY, 2012.
13. Juan Angiolini, Nicolas Plachta, Esteban Mocskos, and Valeria Levi. Exploring the dynamics of cell processes through simulations of fluorescence microscopy experiments. *Biophys. J.*, 108(11):2613–2618, 2015. doi:10.1016/j.bpj.2015.04.014.
14. Masaki Watabe, Satya N. V. Arjunan, Seiya Fukushima, Kazunari Iwamoto, Jun Kozuka, Satomi Matsuoka, Yuki Shindo, Masahiro Ueda, and Koichi Takahashi. A computational framework for bioimaging simulation. *PLoS ONE*, 10(7):e0130089, 2015. doi:10.1371/journal.pone.0130089.
15. Fredrik Persson, Martin Lindn, Cecilia Unoson, and Johan Elf. Extracting intracellular diffusive states and transition rates from single-molecule tracking data. *Nat. Meth.*, 10(3):265–269, 2013. doi:10.1038/nmeth.2367. Software: <http://sourceforge.net/projects/vbspt/>.
16. Winston C. Chow. Brownian bridge. *WIREs Comp. Stat.*, 1(3):325–332, 2009. doi:10.1002/wics.38.
17. Maximilian H Ulbrich and Ehud Y Isacoff. Subunit counting in membrane-bound proteins. *Nat. Meth.*, 4(4):319–321, 2007. doi:10.1038/NMETH1024.
18. A. Finney and M. Hucka. Systems biology markup language: Level 2 and beyond. *Biochem. Soc. T.*, 31(6):1472–1473, 2003. doi:10.1042/bst0311472.
19. S F Gibson and F Lanni. Experimental test of an analytical model of aberration in an oil-immersion objective lens used in three-dimensional light microscopy. *J. Opt. Soc. Am. A*, 9(1):154–166, 1992. doi:10.1364/JOSAA.9.000154.
20. H. Kirshner, F. Aguet, D. Sage, and M. Unser. 3-D PSF fitting for fluorescence microscopy: implementation and localization application. *J. Microsc.*, 249(1):13–25, 2013. doi:10.1111/j.1365-2818.2012.03675.x.
21. William H. Press, Brian P. Flannery, Saul A. Teukolsky, and William T. Vetterling. *Numerical Recipes in C: The Art of Scientific Computing*. Cambridge University Press, Cambridge ; New York, 2 edition, 1992.
22. K. C. Huang, Y. Meir, and N. S. Wingreen. Dynamic structures in Escherichia coli: Spontaneous formation of MinE rings and MinD polar zones. *Proc. Natl. Acad. Sci. U.S.A.*, 100(22):12724–12728, 2003. doi:10.1073/pnas.2135445100.
23. David Fange and Johan Elf. Noise-induced Min phenotypes in E. coli. *PLoS Comput. Biol.*, 2(6):e80, 2006. doi:10.1371/journal.pcbi.0020080.

24. David Fange, Otto G. Berg, Paul Sjberg, and Johan Elf. Stochastic reaction-diffusion kinetics in the microscopic limit. *Proc. Natl. Acad. Sci. U.S.A.*, 107(46):19820–19825, 2010. doi:10.1073/pnas.1006565107.
25. Sang-Hyuk Lee, Jae Yen Shin, Antony Lee, and Carlos Bustamante. Counting single photoactivatable fluorescent molecules by photoactivated localization microscopy (PALM). *Proc. Natl. Acad. Sci. U.S.A.*, 109(43):17436–17441, 2012. doi:10.1073/pnas.1215175109.
26. Andrew J. Berglund. Statistics of camera-based single-particle tracking. *Phys. Rev. E*, 82(1):011917, 2010. doi:10.1103/PhysRevE.82.011917.
27. Hendrik Deschout, Kristiaan Neyts, and Kevin Braeckmans. The influence of movement on the localization precision of sub-resolution particles in fluorescence microscopy. *J. Biophotonics*, 5(1):97–109, 2012. doi:10.1002/jbio.201100078.
28. Johan Elf, Gene-Wei Li, and X Sunney Xie. Probing transcription factor dynamics at the single-molecule level in a living cell. *Science*, 316(5828):1191–1194, 2007. doi:10.1126/science.1141967.
29. Kim I. Mortensen, L. Stirling Churchman, James A. Spudich, and Henrik Flyvbjerg. Optimized localization analysis for single-molecule tracking and super-resolution microscopy. *Nat. Meth.*, 7(5):377–381, 2010. doi:10.1038/nmeth.1447.
30. David MacKay. *Information theory, inference, and learning algorithms*. Cambridge University Press, 2003.
31. Alexandre Lazarescu and Kirone Mallick. An exact formula for the statistics of the current in the TASEP with open boundaries. *J. Phys. A: Math. Theor.*, 44(31):315001, 2011. doi:10.1088/1751-8113/44/31/315001.

Supplementary material

S1 Simulated microscopy with SMeagol

SMeagol is a Matlab software suite that simulates microscopy images of randomly moving particles using two main ingredients: diffusive motion and stochastic photon emission events. In addition, noise from various sources (camera, background, optics, blinking and photobleaching, etc.) can be included in a modular and flexible way. This makes it possible to evaluate how different aspects of the biological-, reporter- and detection- system influence the overall result of the experiment.

Reactions and random motion in arbitrary geometries The microscopy simulation part of SMeagol uses input trajectories in the form of a list of times, positions, particle id numbers, and diffusive states, and can also include the time for creation and destruction of particles. The input trajectories are interpolated using Brownian bridges¹⁶ to generate individual emission positions of every simulated photon. Brownian bridges simulate free diffusion, but the input data need not. Thus, with a fine time step one can use SMeagol to simulate general types of motion. For an example, see Sec. S5b and Fig. S4.

We have extended the reaction-diffusion simulation software MesoRD¹¹ to keep track of individual molecules and write trajectories in the appropriate input format, and incorporated it in SMeagol, but it is also possible to use indata from other sources. SMeagol's trajectory data format is described in the software manual.

Tunable photophysics In parallel with the diffusion process, each particle in the simulation goes through a simulated stochastic photophysical process which includes activation, Markovian transitions between multiple photophysical states with different photon emission intensities, and eventually irreversible photobleaching. Short exposures can be simulated by setting an exposure time t_E shorter than the frame time Δt , and photophysical effects of excitation, by specifying different photophysical transition rates during the illuminated ($0 \leq t < t_E$) and non-illuminated ($t_E \leq t < \Delta t$) phases. Separating photophysics and molecular diffusion makes it possible to simulate the same reaction-motion trajectory under a wide range of experimental conditions.

EMCCD noise and background The emitted photons are mapped to the camera chip using a point-spread function (PSF) model, combined with simulated EMCCD¹⁷ and background noise. The microscopy image, which is written to tif-stacks for further analysis.

Flexible, modular and user-friendly SMeagol is designed to allow easy incorporation of experimental data and theoretical parameters at many levels. Thus, the user can specify arbitrary fluorophore activation and photophysical kinetics, and also incorporate custom-written Matlab routines for PSF and background models, by extending existing template files. It is also possible to use the

independently measured PSF for a specific optical set-up, or background movies from a specific sample. Stochastic reaction-diffusion models are described using the systems biology markup language (SBML)¹⁸ with extensions to spatial models¹¹. The trajectories and the different building blocks of the microscopy simulation are then combined and parameterized using either a graphical user interface, parameter text files (runinput files), or Matlab structs.

S2 Point-spread function (PSF) model

For all microscopy simulations described here, we used a rotationally symmetric PSF model constructed from the Gibson-Lanni model¹⁹, as implemented in PSFgenerator²⁰.

We simulated the Gibson-Lanni PSF model with high resolution for 584 nm light, NA=1.4, and otherwise default settings PSFgenerator, computed the cumulative radial distribution function (CRDF) for different focal planes and radii up to 5 μm , and constructed a Matlab look-up table for the inverse CRDF. An individual photon emitted at $x_{\text{em.}}, y_{\text{em.}}, z_{\text{em.}}$ were then simulated as detected at position

$$x_{\text{det.}} = x_{\text{em.}} + r \cos \nu, \quad (\text{S1})$$

$$y_{\text{det.}} = y_{\text{em.}} + r \sin \nu, \quad (\text{S2})$$

where the angle ν is uniformly distributed on $[0, 2\pi]$, and r is sampled using the inverse transform method²¹, i.e.,

$$r = CRDF^{-1}(u; z_{\text{em.}}), \quad (\text{S3})$$

with u uniformly distributed on $(0, 1)$. The total intensity of the spot did not vary significantly in the region $(|z_{\text{em.}} - z_{\text{focus}}| < 400 \text{ nm})$ relevant for our simulations.

In focus, the above PSF model has a standard deviation of about 335 nm. This is largely due to large shoulders of the PSF, and the width of the central peak is about 95 nm.

S3 Simulated experiments with Min oscillations

To generate Fig. 1c, we simulated a minimal stochastic model of the Min oscillation cycle^{22,23}, implemented using scale-dependent mesoscopic reaction rate constants²⁴.

Reaction-diffusion simulation To match experimental microscopy data, we choose an *E. coli*-like geometry consisting of a cylinder with spherical end caps, with outer diameter 1 μm and total length 2.7 μm . The outer 35 nm of the cell was modeled as the membrane region. In this geometry, the oscillations have a period of 25-30 s.

We used a 10 nm spatial discretization, and initial conditions placing 1716 MinD and 483

MinE randomly in the membrane region at one half of the cell. After a 300 s simulation to reach steady state, we ran a tracking production run, collecting snapshots (used for the left column of Fig 1c) every 0.25 s, and tracking positions of all species involving MinE every 5 ms.

MinE SPT simulation (Fig 1c, mid columns, and supplementary movie S1). We simulated a single particle tracking experiment with 4 ms frame rate and continuous illumination. The coordinate system of the input trajectories were rotated and translated to fit a brightfield image of an *E. coli* bacterium expressing no fluorophores (Fig. 1c), and a fluorescence time-lapse movie of the same cell was used as a background.

The Gibson-Lanni PSF model was used as described above, and an experimentally parameterized blink/bleach model for mEos2²⁵, with a bright state intensity of 125000 photons/s that yields on average 500 photons per spot and 4 ms frame if no blinking occurs. Photoactivation events were simulated every 10 s, with an activation probability of 20% per unconverted molecule.

We simulated an EMCCD gain of 40 (SMeagol inverse gain `camera.alpha=1/40`), i.e., every photon generates an exponentially distributed number of image counts with mean value 40. Offset and readout noise are in this case included in the experimental background.

MinE long-exposure simulation (Fig 1c, right column, and supplementary movie S2). For the long-exposure simulations, we randomly activated 50% of the MinE-containing molecules with a constant emission intensity of 60 photons/s and no blinking or bleaching. For background, we set a uniform intensity of 1 photon/pixel. We used continuous illumination and a frame rate of 1 Hz, the Gibson-Lanni PSF model described above, an EM gain of 40, offset 100, and readout noise with std. 4.

The reaction-diffusion model and trajectory output files, and the SMeagol runinput files for these simulations, are included in Supplementary dataset S1.

S4 Analysis of diffusion with blur and localization errors

To illustrate how SMeagol could be used to evaluate analysis methods for live cell single particle tracking experiments, we explore the ability of the vbSPT software¹⁵ to correctly identify the number of diffusive states in SPT data. We simulated an SPT experiment with normal diffusion at a rate of $D = 1 \mu\text{m}^2 \text{s}^{-1}$ sampled every 3 ms in an *E. coli* geometry with varying fluorophore brightness and exposure time (see Supplementary movie S3). vbSPT assumes that data come from a Markov model with state-dependent diffusion constants, i.e., a model that neglects, e.g., z-dependent localization errors²⁷, motional blur^{26,27}, and confining effects of the cell boundaries. The simulation thus contains many real features not included in the analysis model, which could lead vbSPT to overfit the data by incorrectly identifying more than one diffusive state. The question

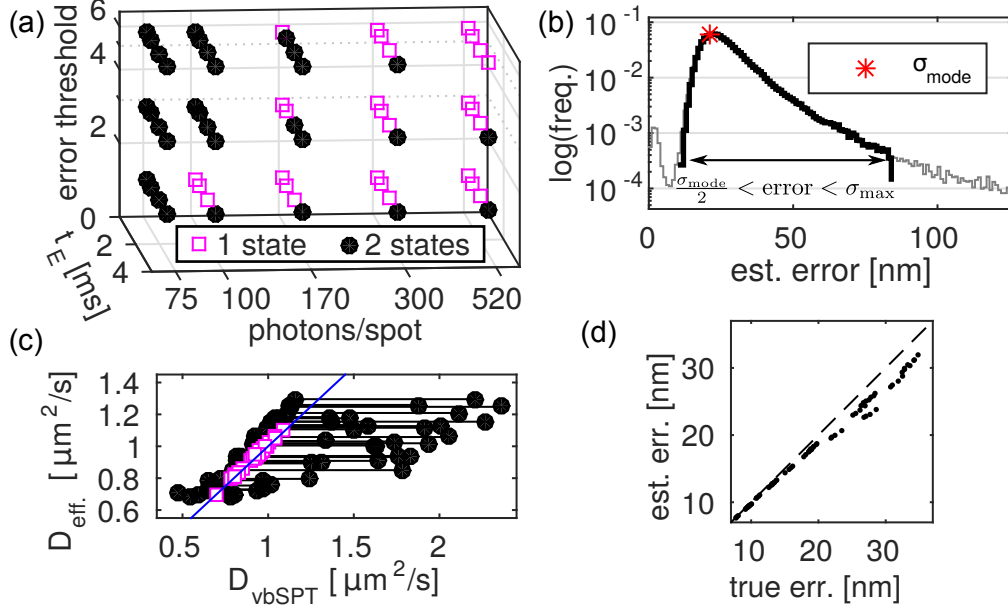


Figure S2: Sensitivity of vbSPT to imaging artifacts. (a) Depending on the experimental parameters, vbSPT correctly finds one diffusive state (pink) or incorrectly finds two diffusive states (black). The experimental parameters are spot intensity, exposure times t_E , and localization error threshold. (b) Spot selection criteria illustrated on a distribution of estimated pointwise localization errors, with $\sigma_{\text{max}}/\sigma_{\text{mode}}$ being the error threshold in (a). (c) Comparison of the diffusion constants found by vbSPT with an effective diffusion constant defined via the theoretical step length variance²⁶. (d) Comparison of the true and estimated (as in (b)) root-mean-square error for every trajectory in (a).

Table S1: Settings for the microscopy simulations of simple diffusion (Fig. S2).

sample time	: 3 ms per frame
photophysics	: constant emission intensity, no bleaching
ROI	: 80 nm pixels, 55×20 pixel ROI, focal plane in the mid- : plane of the bacteria
camera	: offset=100, readout noise std.=4, : EM gain=20 counts/photon
background	: constant, on average 1 photon/pixel per frame

is under which experimental conditions this is likely to happen.

Reaction-diffusion simulation We simulated simple diffusion of a single fluorescent particle in an E coli-like geometry, built as a cylinder with length 3 μm and diameter of 0.8 μm , plus spherical end caps. We used 10 nm voxels, and wrote particle positions every 7 ms.

SMeagol simulation We generated SPT movies with a frame duration of 3 ms in a range of imaging conditions from the above diffusive trajectory, by varying the exposure time t_E and the average number of photons per spot ($N_{phot.} = t_E \times \text{emission intensity}$). In particular, we used all combinations of $t_E = 0.5$ ms, 1 ms, 2 ms, 3 ms, and $N_{phot.} = 75, 100, 300, 520$. Other microscopy parameters used in all cases are summarized in table S1.

Estimated number of states Fig. S2a shows number of states learned by vbSPT as a function of three tuning parameters: the exposure time t_E , the average number of photons per spot, and the maximally allowed pointwise localization error (Fig. S2b). The correct and overfitting conditions are indicated in purple and black, respectively. In general, all three parameters influence the overfitting tendency in a non-trivial way. Continuous illumination (exposure time=frame time) leads to overfitting in almost all conditions, but a modest decrease in exposure time using, e.g., stroboscopic illumination²⁸, leads to significant improvement due to decreased motional blur. We also note that if the number of photons per localized molecule is limited, it is advantageous to include only positions with high localization accuracy.

Estimating the diffusion constant As the analysis model of vbSPT neglects both localization errors and motional blur, one should not take the numerical estimates of the diffusion constants at face value. However, the estimates can be interpreted using a theory of motional blur for diffusing particles²⁶. A closer inspection of the analysis algorithm¹⁵ shows that vbSPT effectively looks at the step length variance, which in the absence of localization error and blur is simply

$$\langle \Delta x^2 \rangle = 2D_{\text{vbSPT}} \Delta t. \quad (\text{S4})$$

A more detailed model that includes motional blur and localization errors²⁶ instead predicts

$$\langle \Delta x^2 \rangle = 2D\Delta t(1 - 2R) + 2\langle \sigma_x^2 \rangle, \quad (\text{S5})$$

where $R = \frac{t_E}{3\Delta t}$ is the motional blur coefficient, and $\langle \sigma_x^2 \rangle$ is the mean-square localization error. Eliminating the step length variance from the above equations, we find that

$$D_{\text{vbSPT}} = D_{\text{eff.}} \equiv D(1 - 2R) + \frac{\langle \sigma_x^2 \rangle}{\Delta t}. \quad (\text{S6})$$

Fig. S2c plots the effective diffusion constant $D_{\text{eff.}}$ vs. the posterior mean of D_{vbSPT} for the different data sets (using our estimated average localization errors), and we see that the prediction of Eq. (S6) is reproduced well when a single diffusive state is correctly identified.

Point localization We localized the spots using a maximum-likelihood fit of a symmetric Gaussian plus constant background to a 7-by-7 fit region, using the EMCCD likelihood function of Ref. 29, with the offset and gain settings of table S1. Each spot is thus described by 5 fit parameters: background b , spot amplitude N , spot standard deviation s , and spot position μ_x, μ_y . We used Matlab's built-in function `fminunc` for numerical optimization of the log likelihood, which was parameterized to allow only positive values of b , N , and s^2 , and used the true spot positions, and the average PSF width and amplitude to construct an initial guess for each fit. To minimize confinement artifacts from the cell walls, we analyzed motion and uncertainties along the long cell axis (x coordinate) only.

Estimating point-wise localization uncertainty Due to fluorophore motion during exposure, random photon emission, z -dependence of the PSF, etc., the quality of the fit varies from spot to spot. We used a Laplace approximation³⁰ (also known as the saddle point approximation in statistical physics) of the likelihood function to estimate the localization uncertainty of individual spots, as follows: Let IM denote the fit region of the image used for localization, and $\theta = (\mu_x, \mu_y, \dots)$ the fit parameters. We approximate the likelihood function $p(IM|\theta)$ by a Gaussian centered at the maximum likelihood estimate θ^* using a Taylor expansion in $(\theta - \theta^*)$,

$$p(IM|\theta) \approx \exp \left(\underbrace{\ln p(IM|\theta^*) + \nabla_{\theta} \ln P(IM|\theta)|_{\theta^*}}_{=0} (\theta - \theta^*) - \frac{1}{2}(\theta - \theta^*)^T \Sigma^{-1} (\theta - \theta^*) + \dots \right), \quad (\text{S7})$$

where the first order term disappears since θ^* is a local maximum, and the second order term is given by the inverse covariance matrix,

$$\Sigma^{-1} = - \frac{\partial^2 \ln p(IM|\theta)}{\partial \theta^2} \Big|_{\theta^*}. \quad (\text{S8})$$

This can be interpreted as the Bayesian posterior distribution (with a flat prior). The uncertainty of the parameters are then characterized by their posterior covariances³⁰. In particular, the posterior variance of μ_x is approximately given by Σ_{μ_x, μ_x} .

As a simple test of this estimator, we compare the true and estimated average root-mean-square (RMS) error for all points in every trajectory (Fig. S2d). We find it to be correct on average, i.e.,

$$\langle (\mu_x^* - \mu_{x,\text{true}})^2 \rangle \approx \langle \Sigma_{\mu_x, \mu_x} \rangle, \quad (\text{S9})$$

for true RMS errors $\lesssim 20$ nm, but biased downwards for larger errors, probably because the Gaussian approximation of the posterior density (Eq. (S7)) is inaccurate in those cases.

Selection criteria To build diffusion trajectories for vbSPT analysis, we first discarded spots where the numerical optimization failed. We then built a histogram of estimated standard errors $\sigma_x = \sqrt{\Sigma_{\mu_x, \mu_x}}$, and identified the most likely estimated error σ_{mode} . One such histogram is shown in Fig. S2b. Finally, we discarded spots that had either $\sigma_x < \sigma_{\text{mode}}/2$ as being unrealistically precise, or $\sigma_x > \sigma_{\text{mode}} \times (\text{error threshold})$, using error thresholds in the range 1.3 – 6 as our third control variable in Fig. S2a. The highest threshold of 6 included practically all spots.

The fraction of retained spots as well as average trajectory length vary with both simulation parameters and error threshold, but for this experiment we generated enough images to construct data sets with 80 000 diffusive steps for all conditions.

vbSPT settings For the trajectory analysis, we used vbSPT 1.1.2¹⁵. For each data set, we ran 20 independent runs of the greedy model search algorithm with up to 15 hidden states. We used an inverse gamma prior with mean value $1 \mu\text{m}^2 \text{s}^{-1}$ and strength 5 (std. $\approx 0.6 \mu\text{m}^2 \text{s}^{-1}$) for the diffusion constants (with 80 000 diffusive steps in the trajectory, this prior is completely overwhelmed by the data), flat Dirichlet priors for the initial state and state-change probability distributions, and a Beta distribution with mean 0.02 s and std. 2 s for the mean dwell time of the hidden states. (For detailed definitions, we refer to the vbSPT manual).

S5 Misc. model examples

Here, we briefly describe some additional model examples, to illustrate the capability and limitations of SMeagol in various settings. Source files for these examples are included in Supplementary data S5.

S5a. Affinity to cell poles To illustrate the geometric modeling capabilities of MesoRD and SMeagol, we construct a simplified model of a diffusing cytoplasmic protein P with specific affinity to binding partners localized at the cell poles.

We use an E coli-like rod shape, where cytoplasm is modeled by a union of a cylinder and two spheres with radii 465 nm. In the cytoplasm, the proteins diffuse with diffusion constant $2.5 \mu\text{m}^2 \text{s}^{-1}$. The membrane region is modeled as an additional 35 nm outer shell, from which polar regions in the form of small spherical caps are created, as shown in Fig. S3a. In these

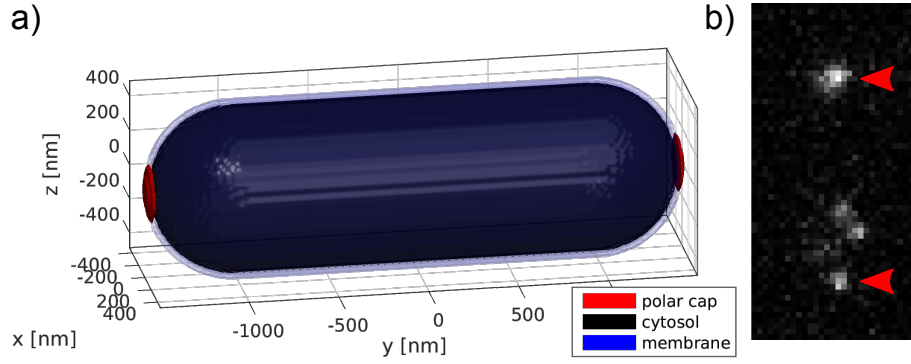


Figure S3: Simulating a diffusing protein with polar binding regions. a) Model geometry, with the cytosol (black) inside a thin membrane region (blue) that also contains polar caps (red,magenta) where binding receptors are localized. b) Snapshot from a simulated SPT experiment, with both polar bound (red arrows) and freely diffusing molecules visible.

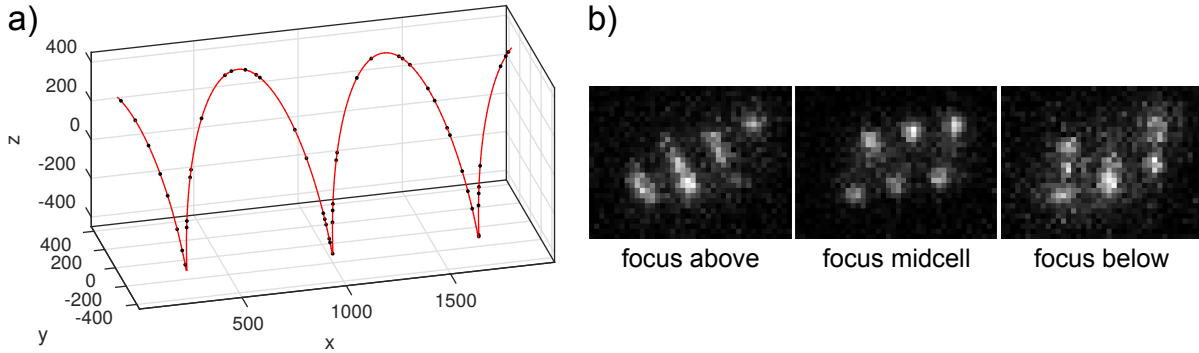


Figure S4: Simulating non-diffusive transport. (a) Snapshot from TASEP simulation (black, particles) on a helical path (red). (b) Simulated images with focal plane placed near the upper, middle, and lower part of the helical curve emphasize different parts of the path.

caps, we assume a constant concentration $[R]$ of receptors. Then, the binding rate can be written $r = k_a[R][P]$, where k_a is the association rate constant, and the unbinding rate constant is k_d . We choose $k_a[R] = 20 \text{ s}^{-1}$, $k_d = 0.01 \text{ s}^{-1}$, and diffusion constant $0.01 \mu\text{m}^2 \text{ s}^{-1}$ for the bound complex (confined to the membrane caps).

We ran 6 s of stochastic reaction-diffusion simulations starting with 125 P molecules uniformly distributed outside the polar caps, and after a burn-in of 2 s, wrote positions to file every 1 ms. For the microscopy simulation, we randomly activated 5% of the molecules, and used the same settings as in the simple diffusion experiment above (table S1), except slightly larger region of interest, a fluorophore intensity corresponding to giving on average 270 photons/frame and fluorophore, and photobleaching with a mean lifetime of 1 s. A snapshot is shown in Fig. S3b.

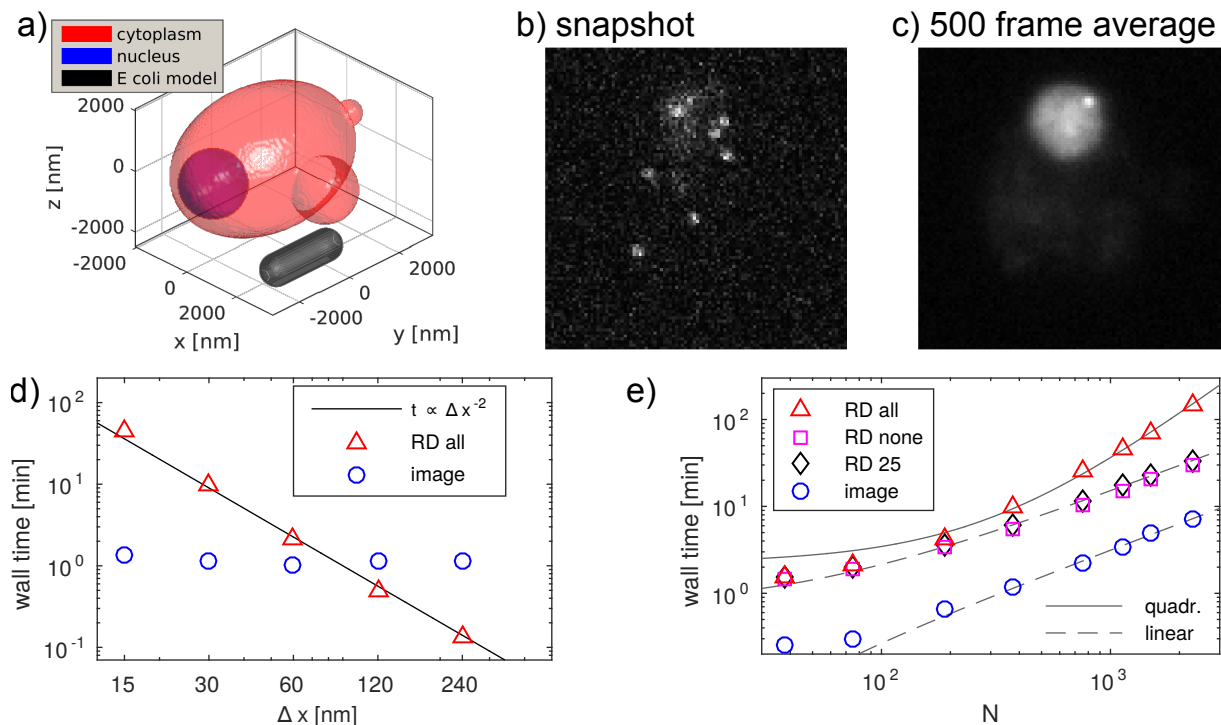


Figure S5: Simulating a diffusing transcription factor in a yeast cell. (a) The model geometry includes a cytoplasm compartment with two buds (red) and a spherical nucleus (blue). Also shown is the bacterial model of Fig. S3 (black). (b,c) A snapshot and 500-frame average, respectively, from a 5 ms/frame SPT simulation. (d) Wall time versus voxel size for a 5 s stochastic reaction diffusion simulation tracking all proteins (RD all), and microscopy image simulation. The former closely follows the expected $1/\Delta x^2$ scaling, while the latter is essentially constant. (e) Wall times for the $\Delta x = 30$ nm case from (d), but with varying number of involved proteins. “RD none” and “RD 25” refers to stochastic reaction diffusion simulations with tracking deactivated and tracking only 25 proteins irrespective of total copy number.

S5b. Non-diffusive transport along helical membrane filaments To illustrate the possibility of simulating more complex motion than diffusion using SMeagol, we constructed an active transport model of particles moving on a helical path (Fig. S4). More specifically, we wrote a Matlab script to simulate a totally asymmetric exclusion process (TASEP³¹) with open boundaries: Particles (black) are created at the left end of the helix in Fig. S4a, walk forwards in 36 nm steps along the helical path (red) with a rate of 10 s^{-1} (under a site exclusion constraint), until they fall off at the right end. The insertion rate was 2 s^{-1} , putting the TASEP in the low density phase³¹. We then wrote particle coordinates to a trajectory text file at regular intervals (all in the same chemical state), and fall-off events as particle destructions in the reactions text file. For microscopy simulations, we set $D = 0$, which disables the Brownian bridges and leads to linear interpolation between the trajectory coordinates. Simulation scripts and runinput files are included in data set S5.

S5c. A large cell To illustrate the computational requirements of SMeagol, we use a simple model of transcription factor (TF) motion in a budding yeast cell. The model has a cytoplasmic compartment, made of two spheres joined to an ellipse with a spherical nucleus compartment inside. As seen in Fig. S5a, it is several times larger than the bacterial-like examples described so far.

The main computational load for fine-scale MesoRD simulations consists of diffusive motion (total diffusive hopping rate is $6D/\Delta x^2$), so we use a simple kinetic model where the TF has a 'free' state that diffuses with diffusion constant $2.5 \mu\text{m}^2 \text{s}^{-1}$ in the entire cell, and can interconvert to a 'bound' state ($0.01 \mu\text{m}^2 \text{s}^{-1}$) inside the nucleus. In addition, we simulate active transport into the nucleus by setting the diffusion rate from the cytoplasm to the nucleus 20 times larger than that in the reverse direction. Protein accumulation in the nucleus is clearly visible in the simulated images (Fig. S5b,c).

Fig. S5d shows wall time¹ for a 5 s stochastic reaction-diffusion simulation, starting with about 375 uniformly distributed TFs and various voxel sizes, which fits very well with the expected inverse quadratic scaling $\propto \Delta x^{-2}$. Second, we generated a 2.5 s simulated microscopy movie with 5 ms frame time, 100 80 nm pixels, and 10% of the proteins activated and emitting on average 270 photons/frame. This simulation is limited by evaluating Brownian bridges and parsing the trajectory file, and thus independent of the discretization of the trajectories.

Secondly, we varied the number of proteins, while keeping the discretization constant at $\Delta x = 30 \text{ nm}$. As seen in Fig. S5d, the image simulation part scales linearly as expected, while the RD simulation scales quadratically if all proteins are tracked, but linearly with tracking deactivated or if tracking only a fixed number of proteins. Thus, we see that while fairly large cells can be simulated, the RD simulations can be computationally demanding especially for models that include large cell size, tracking of many molecules, and small details that require fine discretizations.

Finally, we note that the total size in itself does not influence computing time significantly, as long as the number of subvolumes fit in the RAM memory of the computer. As an illustration, we rescaled all length in the $\Delta x = 30 \text{ nm}$ case of Fig. S5d by a factor 0.3 (thus decreasing the volume by 97%) but kept the discretization and number of molecules constant. However, the RD simulation of the smaller model only took 25% less time.

S5d. Complex shapes To highlight SMeagol's abilities to model geometries beyond the tractable possibilities given by transformation and combinations of simple geometric primitives, we also model particle diffusion in an erythrocyte shaped geometry, shown in Fig. S6a. The starting point is here a freely available 3D model², which we imported to and exported from Blender³ to make

¹All computing times were measured on a 2.40GHz Intel Xeon CPU with 24 GB RAM.

²<http://www.turbosquid.com/FullPreview/Index.cfm/ID/509576>, accessed 2016-02-04)

³www.blender.org

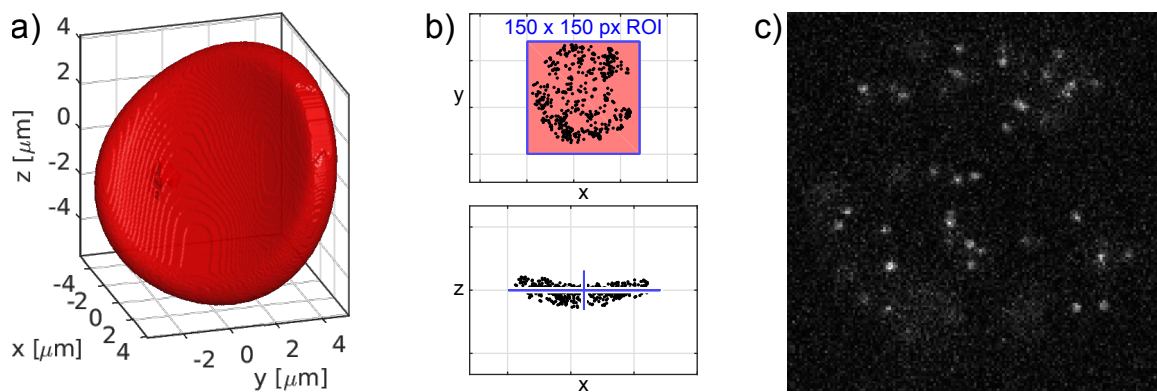


Figure S6: Modeling an erythrocyte. a) Rendering of the SBML model with 50 nm subvolumes. b) Alignment of the model (particle positions indicated by black dots) relative to the simulated region of interest (ROI) and focal plane of the simulation. c) Snapshot from a simulated movie with 25 ms exposure time.

it a triangular mesh. The mesh was then converted to SBML compatible format using a custom Python script, and incorporated into an SBML model, where about 70 particles diffuse freely ($D=2 \mu\text{m}^2 \text{s}^{-1}$) within the erythrocyte.

For the microscopy simulation, we rotated the model to align it with the focal plane as shown in Fig. S6b and used similar settings as for the yeast example to produce the snapshot in Fig. S6c.

S6 Misc. supplementary material

- **Supplementary movie S1** illustrates the simulated MinE single particle tracking experiment (Fig. 1c, mid columns), showing both true particle positions, the experimental background, and the simulated result in three separate panels.
- **Supplementary movie S2** illustrates the simulated MinE fluorescence microscopy time-lapse movie (Fig. 1c, right column), as well as the true particle positions.
- **Supplementary movie S3** shows simulated single particle tracking experiments that are analyzed in Fig. S2.
- **Supplementary dataset S4** contains the SBML files, reaction-diffusion trajectory output, and SMeagol runinput files for the simulated Min oscillation experiments (Fig. 1c).
- **Supplementary dataset S5** contains model and runinput files, scripts, and source files for the example models described in Sec. S5.